Investigation of the Mechanism of Intracluster Proton Transfer from Sinapinic Acid to Biomolecular Analytes

C. M. Land and G. R. Kinsel
Department of Chemistry and Biochemistry, University of Texas at Arlington, Arlington, Texas, USA

Experiments have been performed to elucidate the mechanism of proton transfer in ternary clusters containing the matrix-assisted laser-desorption ionization (MALDI) matrix sinapinic acid, nonchromophoric analytes (proline, methionine, and prolylmethionine), and argon. To investigate the mechanism of intracluster proton transfer, ionizing laser power studies were performed at 266 and 355 nm. Baseline studies show that two photons are required at both wavelengths for the formation of sinapinic acid radical cations from sinapinic acid/argon clusters. Studies of the ternary sinapinic acid/biomolecule/argon clusters show that, in all cases, the photon dependence for protonation of the biomolecule is the same as that for formation of the sinapinic acid radical cation. Furthermore, the slopes of the power plots are generally between 1.5 and 2.0, consistent with a two photon ionization process. No evidence of negative ion formation is detected in the negative ion mass spectra. The combined results are consistent with a mechanism of biomolecular intracluster protonation via proton transfer from the photoionized sinapinic acid radical cation. Wavelength dependent trends in matrix and analyte fragment ion formation in conventional MALDI mass spectra and the cluster proton transfer mass spectra were noted. The possible contribution of cluster proton transfer to the analyte protonation mechanism in conventional MALDI is discussed. (J Am Soc Mass Spectrom 1998, 9, 1060–1067) © 1998 American Society for Mass Spectrometry

Achieving an improved understanding of the mechanism and dynamics of analyte ionization during matrix-assisted laser desorption ionization (MALDI) [1–4] remains an important goal. Specifically, given that protonation is the dominant analyte ionization pathway, it is desirable to clarify the requirements for a potential matrix molecule to act as a proton source for a given analyte or class of analyte molecules. This parametrization could substantially accelerate the discovery of new MALDI matrices and allow MALDI mass spectrometry to be more effectively employed in the analysis of a broader spectrum of biological and nonbiological macromolecules. Furthermore, thorough characterization of the MALDI ion formation dynamics could reveal new approaches for producing higher ion signal resolutions, more reproducible ion signal intensities, and/or improved limits of detection.

This goal has inspired a wide variety of studies of both the mechanism and dynamics of MALDI analyte ionization. Studies of the analyte ionization mechanism have focused on elucidating the role of various analyte ionization pathways including matrix to analyte excited state proton transfer, matrix radical cation to analyte proton transfer, and protonated matrix to analyte proton transfer [5–11]. Both theoretical and experimental studies continue to provide new insights into the MALDI analyte ionization mechanism and these results have been interpreted with regard to the various postulated mechanisms of analyte ionization [12–17]. Studies of the dynamics of ion formation continue to address both the kinetic energy distribution and temporal evolution of the MALDI ions with interpretation of the results in terms of both condensed phase and gas-phase analyte ionization processes [18–22]. However, despite these ongoing experimental efforts, a comprehensive picture of the MALDI desorption and ionization process has not yet emerged.

Within the context of developing novel methods to probe the MALDI analyte ionization process, a small group of researchers have investigated matrix to analyte proton transfer reactions occurring in neutral matrix/analyte clusters [23–26]. In these studies the clusters are formed by seeding the matrix and analyte molecules into a supersonic jet expansion and intracluster dissociative proton transfer between the matrix and analyte molecules is initiated by laser photoexcitation of the cluster in the source region of a time-of-flight (TOF) mass spectrometer. These studies are of interest for two reasons. First, it can be readily argued that cluster proton transfer may play a role in the MALDI analyte ionization process since the formation of small matrix/analyte clusters might be expected during the laser

Address reprint requests to Dr. G. R. Kinsel, Department of Chemistry and Biochemistry, The University of Texas at Arlington, P. O. Box 19065, Arlington, TX 76019-0065. E-mail: kinsel@uta.edu

1044-0305/98/$19.00
PII S1044-0305(98)00070-1

Received November 18, 1997
Revised May 14, 1998
Accepted May 14, 1998

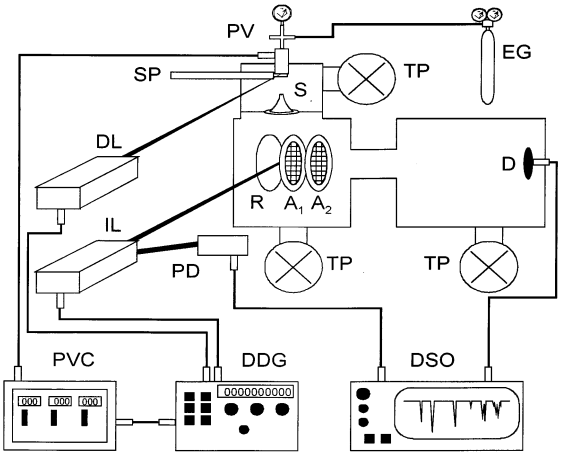

Figure 1. Schematic representation of the cluster TOF mass spectrometer (see text for details). PV = pulse valve, SP = sample probe, EG = expansion gas, S = skimmer, R = repeller plate, A_1 = first acceleration grid, A_2 = second acceleration grid, D = detector, TP = turbomolecular pump, DL = desorption laser, IL = ionization laser, PD = photodiode, PVC = pulse valve controller, DDG = digital delay generator, DSO = digital storage osciloscope.

induced phase transition. Second, studies of the mechanism of matrix to analyte cluster proton transfer are considerably simplified over conventional MALDI because the ionization process is probed independent of the laser desorption event.

We report here the results of our studies of the mechanism of 266 and 355 nm dissociative cluster proton transfer (CPT) in small clusters of the MALDI matrix sinapinic acid with analytes proline, methionine, and prolylmethionine. These studies provide clear evidence that matrix to analyte CPT is initiated by the formation of a matrix radical cation. However, assessment of the relative importance of CPT to MALDI analyte ionization through comparisons of the CPT and conventional MALDI mass spectra remains uncertain.

Experimental

Cluster TOF Mass Spectrometer

A schematic representation of the instrument used for the cluster studies is shown in Figure 1. The instrument consists of a supersonic jet expansion chamber, where clusters of the matrix and analyte molecules are formed, attached to a home-built linear TOF mass spectrometer. To create the matrix/analyte clusters a dry mixture of the two materials is applied to a sample probe (SP) and inserted through a vacuum interlock into the differentially pumped jet chamber. The sample is then illuminated with the defocused, 4-ns duration, 266-nm output of a pulsed Continuum Minilite (Santa Clara, CA) Nd:YAG laser (DL) resulting in resonant desorption of the chromophoric sinapinic acid and codesorption of the nonchromophoric analyte. Typical fluences used for laser desorption of the matrix/analyte mixture are $\sim$900 J/m^2. Laser desorption of the sample occurs 2 mm downstream from the 800 μm opening of a General Valve (Fairfield, NJ) Series 9 pulse valve (PV). Immediately following laser desorption of the sample mixture, the pulse valve is opened for 500 μs, allowing a pulse of pure Ar (EG, 8–9 atm backing pressure) to enter the high vacuum of the jet chamber and intersect the desorbed sample plume. During the "on" portion of the pulse valve cycle, the pressure in the chamber rises from a baseline of 1×10^{-6} to 1×10^{-4} torr. The collision of the expanding gas with the desorbed sample results in entrainment and collisional cooling of the desorbed material followed by molecular cluster formation. The clustered material is skimmed 10 mm downstream of the pulse valve nozzle using a stainless steel Beam Dynamics (Minneapolis, MN) skimmer (S) with an orifice diameter of 780 μm.

The resulting beam of clusters enters a second high vacuum chamber and travels an additional 13 cm before arriving at the center of the source region of a TOF mass spectrometer between the repeller (R) and first acceleration (A_1) electrodes. Opening of the pulse valve causes the source region pressure to increase from a baseline of 1×10^{-8} to 5×10^{-6} torr. The 360 and 120 L/s turbomolecular pumps (TP) on the source region and flight tube, respectively, recover baseline vacuum at the duty cycle of 4 Hz used in these experiments. The repeller, first acceleration and second acceleration (A_2) electrodes of the source region are maintained at positive potentials of 5.2, 4.7, and 0.0 kV, respectively, throughout the experiment. Continuous biasing of the source region in this manner prevents charged ions or clusters formed during the desorption step from entering the TOF mass spectrometer source region.

Ionization of the neutral clusters and molecules which enter the TOF mass spectrometer source region is achieved using the pulsed 355 or 266 nm output of a Continuum Surelite (Santa Clara, CA) Nd:YAG laser (IL). The output of the ionization laser enters through a quartz window located on the side of the TOF mass spectrometer source chamber, passes through the center of the source region and exits through a second quartz window on the opposite side of the source chamber. The direction of propagation of the laser pulse is orthogonal to both the cluster beam axis and the TOF mass spectrometer axis. The output of the ionization laser is focused with a spherical, plano-convex lens (f.l. = 450 mm at 355 nm), located 170 mm from the centerline of the TOF mass spectrometer axis. Using this approach, molecules and clusters are irradiated with a nearly uniform intensity cylindrical beam having diameters of $\sim$6.9 and 7.4 mm at 266 and 355 nm, respectively. (Using simple geometric optical approximations, the variation in laser intensity across the ion formation/collection zone in the TOF mass spectrometer source region is estimated to be less than 5%.) Ionization laser energies are determined by measuring the laser energy both before entering and after exiting the TOF mass spectrometer source region using a coherent fieldmaster energy meter. The average total energy loss due to the

two quartz windows is 30% and 25% at 266 and 355 nm, respectively, leading to calculated energy losses per quartz window of 17.3% at 266 nm and 13.8% at 355 nm. During a given experiment the laser energy at the point of ionization is determined by measuring the laser energy exiting the source region and correcting the value for the energy loss at the second source region window. Ionization laser energies determined in the fashion described, the estimated beam diameters given above, and a value of 5 ns for the ionization laser pulse duration were used to calculate all laser powers reported.

The resulting positively charged ions formed by the ionization laser pulse are accelerated and detected at the end of a 1 m flight tube with a Galileo (Sturbridge, MA) dual microchannel plate detector (D). All TOF mass spectra are recorded and signal averaged on a 500 MHz LeCroy (Chestnut Ridge, NY) 9350AM digital storage oscilloscope (DSO) triggered by a photodiode (PD) that is positioned to detect a reflection of the ionization laser pulse. Timing of the sequence of experimental events is initiated by using the synchronized output of the Iota One (General Valve Corp., Fairfield, NJ) pulse valve controller (PVC) as a master trigger for a Stanford Research (Sunnyvale, CA) DG535 digital delay generator (DDG). Two outputs of the digital delay generator are used to provide triggers for firing of the desorption and ionization lasers and are adjusted to optimize the yield of protonated analyte ion signals. Delays of 110 μs between pulse valve and desorption laser triggers and 270 μs between desorption laser and ionization laser triggers are typically employed.

MALDI TOF Mass Spectrometer

All MALDI mass spectra were acquired using a home-built linear TOF mass spectrometer with a 1.0 m field-free drift tube. Samples are prepared by depositing matrix and analyte onto an electrically isolated 6-mm-diameter nipple on the surface of stainless steel sample probe. Once prepared, the sample containing probe enters the TOF source region from behind the repeller electrode which is biased at 18 kV. The sample containing nipple projects through a hole in the center of the repeller electrode so that the surface of the nipple is flush with the surface of the repeller electrode. Matrix and analyte ions produced by pulsed laser irradiation of the sample are accelerated across the 18.0 kV/cm electric field and enter the field-free drift region. At the end of the field-free drift region the ions are postaccelerated an additional 4.0 kV across a 10 mm distance before striking the surface of a triple microchannel plate detector (R. M. Jordan, Grass Valley, CA, Model C-0701). Transient currents from the ion packets striking the detector are recorded on a 500 MHz digital storage oscilloscope (LeCroy 9350 AM) which is initially triggered by the synchronous output from the desorbing laser. All MALDI mass spectra are typically signal averaged for 50 laser shots.

Pulsed desorbing laser radiation is provided by the frequency tripled (355 nm, 4 ns duration) and quadrupled (266 nm, 4 ns duration) output of a Continuum Minilite (Santa Clara, CA) Nd:YAG laser. At each wavelength the desorbing laser radiation is focused onto the surface of the sample probe using a plano-convex, fused silica lens (nominal focal length of 250 mm) at an angle of 60° relative to the sample surface. In typical operation the distance between the focusing lens and the sample is adjusted to account for the change in focal length at the two wavelengths employed in these studies. This allows approximately equal areas of the sample surface to be irradiated at either wavelength used. In addition, the incident laser energy is controlled using a rotatable neutral density filter wheel positioned in the beam path of the Nd:YAG laser and adjusted to fluences near threshold for observation of the protonated analyte molecule. Typical laser fluences used for MALDI mass spectrometry are approximately 240 J/m^2 (30 μJ/pulse) and 560 J/m^2 (70 μJ/pulse) at 266 and 355 nm, respectively.

Sample Preparation

Sinapinic acid (SA), methionine (M), and prolylmethionine (PM) were purchased from Sigma (St. Louis, MO) and used as received. Proline (P) was purchased from Aldrich (Milwaukee, WI) and used as received. Samples for MALDI mass spectrometry are prepared by codepositing the SA (2 μL of a 10 mg/mL solution in methanol) and analyte (2 μL of a 1 mg/mL solution in water) and allowing the matrix and analyte to cocrystallize in air on the stainless steel sample probe. This somewhat lower than conventional matrix to analyte ratio was used to more closely reflect the matrix to analyte ratios employed in the CPT studies. Samples for CPT TOF mass spectrometry are prepared by mixing equal masses of solid matrix and analyte (typically 1–2 mg of each) mechanically and affixing the solid mixture to the surface of the stainless steel sample probe using a commercial solid adhesive.

Results

Cluster Proton Transfer Mass Spectra

Figures 2 and 3 present positive ion TOF mass spectra resulting from the 355 and 266 nm photoexcitation of clusters of P+SA, M+SA, and PM+SA formed in supersonic jet expansions of argon. Expansions of the SA parent ion region are shown to the right of the corresponding mass spectrum. In these experiments the numbers of analyte molecules, sinapinic acid molecules, and argon atoms making up the initial distribution of neutral clusters is not controlled. However, experiments performed in our laboratory suggest that, under the described experimental conditions, the clusters are likely made up of many molecules and atoms of each of the three components [27]. Negative ion TOF mass

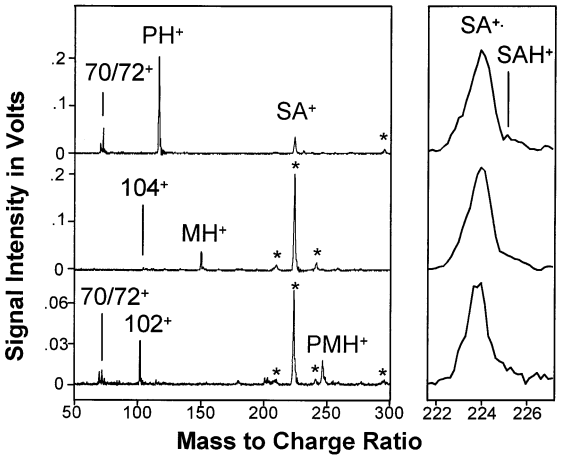

Figure 2. Positive ion mass spectra resulting from 355 nm excitation of clusters containing argon, sinapinic acid, and (**a**) proline, (**b**) methionine, and (**c**) prolylmethionine. Each mass spectrum is the average of 50 laser shots taken at an ionization laser power of 5.5 MW/cm^2. Expansions of the corresponding matrix parent ion region is shown to the right of each mass spectrum.

spectra were also recorded for each of the wavelengths and sample mixtures. These mass spectra showed no ion signals assignable to either the SA or the analyte molecules.

In the mass spectra shown, fragment and cluster ions originating from the SA (as identified by taking background mass spectra of pure SA) are indicated by asterisks. Fragment ions of SA are generally reduced in the 355 nm CPT mass spectra as compared with the 266 nm mass spectra despite the higher ionization laser powers used at 355 nm. Note also that the m/z 180 SA fragment ion exhibits strong ion signals in only the 266

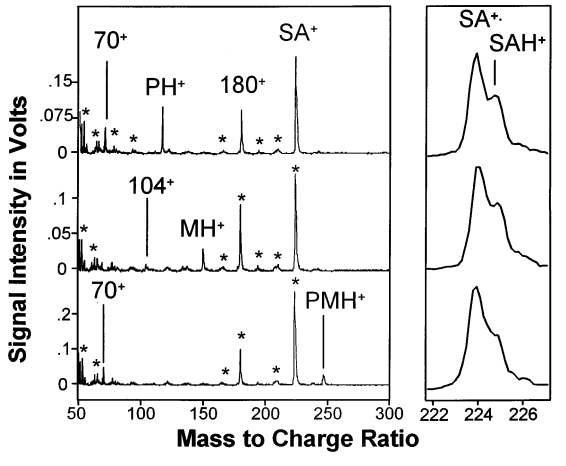

Figure 3. Positive ion mass spectra resulting from 266 nm excitation of clusters containing argon, sinapinic acid, and (**a**) proline, (**b**) methionine, and (**c**) prolylmethionine. Each mass spectrum is the average of 50 laser shots taken at an ionization laser power of 0.73 MW/cm^2. Expansions of the corresponding matrix parent ion region is shown to the right of each mass spectrum.

nm mass spectra. The maximum intensity of the SA parent ion signal corresponds to that of the SA^+ in both the 355 and 266 nm CPT mass spectra. However, a sizable contribution to the parent ion signal from the protonated SA is observed in the 266 nm mass spectra that is not observed in the 355 nm mass spectra.

Protonated biomolecule ion signals are observed for P, M, and PM in both 355 and 266 nm CPT mass spectra. Fragment ion signals at both m/z 70 and 72 are observed in the 355 nm CPT mass spectra of P and PM, whereas the m/z 72 fragment ion signal is absent in the 266 nm CPT mass spectra. The ratio of the m/z 70 fragment ion signal relative to the protonated P and PM parent ion signals also increases as the ionization wavelength is changed from 355 to 266 nm. A large fragment ion signal at m/z 102 is observed in the 355 nm CPT mass spectra of PM that is not observed in the 266 nm CPT mass spectra. Finally, in the CPT mass spectra of M, a fragment ion signal at m/z 104 is observed when using either 355 or 266 nm ionization wavelengths and its intensity relative to MH^+ is essentially independent of the wavelength.

Cluster Proton Transfer Laser Power Studies

In subsequent studies the intensities of the ion signals associated with the protonated analyte and the SA radical cation were examined as a function of ionizing laser power. Studies of this type have previously been employed to indicate the number of photons required to produce a given ion from both small clusters and aerosol particles [28, 29]. Initially, these power studies were performed on clusters of pure, laser-desorbed SA and Ar using 266 and 355 nm laser ionization. In these studies 10 shot mass spectra were acquired at a repetition rate of 4 Hz with 1 min delays between each mass spectrum. Preliminary studies showed that this approach allows the introduction of constant number densities of SA and analyte to the TOFMS source region (i.e., under constant ionization conditions the SA radical cation and protonated analyte ion signals vary by less than 20% relative standard deviation over several hundreds of laser shots). In addition, the ionizing laser power was varied randomly from high to low laser power to minimize systematic sample depletion effect on the $SA^{+\cdot}$ ion signal. Figure 4 shows plots of the log of the $SA^{+\cdot}$ ion signal intensity versus the log of the 266 and 355 nm ionization laser power. Note that the yield of $SA^{+\cdot}$ is lower at 355 nm, despite the somewhat higher SA molar absorptivity (ϵ^{266} = 2600 M^{-1} cm^{-1}, ϵ^{355} = 2800 M^{-1} cm^{-1} in methanol). The data shown represent the average of three separate power studies taken using three separate laser desorption spots. The slopes of the plots are 1.9 ± 0.1 and 2.0 ± 0.2 at 266 and 355 nm, respectively (see Table 1).

Following the studies of the pure SA clusters, the described approach was used to examine the 266 and 355 nm ionizing laser power dependence of the $SA^{+\cdot}$ and $(analyte+H)^+$ ion signals resulting from 266 nm

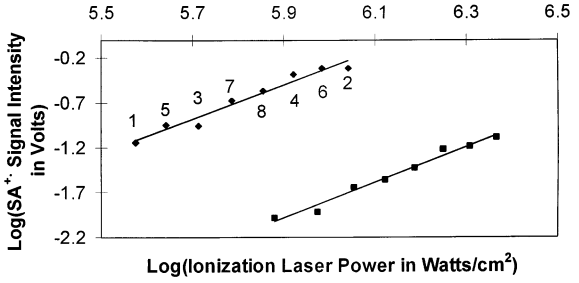

Figure 4. Example of the ionizing laser power plots for laser excitation of clusters of sinapinic acid and argon. The plot of the log of the intensity of the sinapinic acid radical cation signal vs. the log of the ionizing laser power gives linear least square slopes (see Table 1) of 1.9 at 266 nm (diamond) and 2.0 at 355 nm (square). For all power plots the order in which the mass spectra are taken is varied randomly to minimize systematic errors due to depletion of the sample. (The order of mass spectrum acquisition is indicated numerically for the 266 nm study.)

laser desorption of samples of P+SA, M+SA, and PM+SA. Note that P, M, and PM do not absorb efficiently ($\epsilon < 5\ M^{-1}\ cm^{-1}$) at either the 266 or 355 nm laser excitation wavelength. In addition, it should be pointed out that studies of pure samples of the analyte yield no discernible ion signals at ionizing laser energies up to 20 times greater than those used for the mixed SA/analyte clusters. Table 1 gives the average slopes and standard deviations of the three individual runs making up the complete power study for each of the systems investigated. The slopes for formation of $SA^{+\cdot}$ are shifted from the values of 1.9 and 2.0 observed for the pure SA sample to values between 1.4 and 2.0 in the SA+analyte cluster systems. With the exception of 266 nm CPT ionization of $(PM+H)^+$, the slopes of the power plots for the formation of the protonated analyte ions are between 1.6 and 2.0.

In addition, the ionizing laser power dependent changes in the ratio of the $(analyte+H)^+$ to $SA^{+\cdot}$ ion signal intensities were examined. Table 2 lists the slopes and standard deviations of plots of the $(analyte+H)^+/SA^{+\cdot}$ ion signal intensity ratio versus the 266 and 355 nm ionization laser power. The values shown are not simply the ratios of the power plot slopes for each of the two individual ions, but instead are the slopes of the power plots derived from the actual ratio of the signal intensities in each spectrum. As shown in Table 2 the slopes of these plots range from −0.31 to +0.49.

Table 1. Average slopes obtained from plots of the $log[SA^{+\cdot}]$ and $log[(analyte)H^+]$ vs. log[ionization laser power] for 355 and 266 nm photoexcitation of clusters of SA or SA plus analyte in argon. The values listed are the average and standard deviation of the results from three separate ionizing laser power studies for each set of conditions indicated

	355 nm ionization		266 nm ionization	
System	$SA^{+\cdot}$	$(Analyte)H^+$	$SA^{+\cdot}$	$(Analyte)H^+$
SA	2.0 ± 0.2		1.9 ± 0.1	
P+SA	1.5 ± 0.3	2.0 ± 0.4	1.4 ± 0.3	1.6 ± 0.5
M+SA	1.9 ± 0.3	1.7 ± 0.4	1.6 ± 0.2	1.9 ± 0.2
PM+SA	1.7 ± 0.3	1.7 ± 0.2	1.6 ± 0.1	1.2 ± 0.1

Table 2. Average slopes obtained from plots of the $log[(analyte)H^+/SA^{+\cdot}]$ vs. log[ionization laser power] for 355 and 266 nm photoexcitation of clusters of SA plus analyte in argon. The values listed are the average and standard deviation of the results from three separate ionizing laser power studies for each set of conditions indicated

	355 nm ionization		266 nm ionization	
Ratio	Slope	Standard deviation	Slope	Standard deviation
$PH^+/SA^{+\cdot}$	0.49	0.24	0.12	0.20
$MH^+/SA^{+\cdot}$	−0.25	0.25	0.28	0.25
$PMH^+/SA^{+\cdot}$	0.06	0.28	−0.31	0.20

MALDI Mass Spectra

Figures 5 and 6 present positive ion 355 and 266 nm MALDI mass spectra of P, M, and PM with SA as the matrix. Expansions of the SA parent ion region are shown to the right of the corresponding mass spectrum. In these mass spectra fragment and cluster ions originating from the SA are indicated by asterisks. Similar to the results of CPT mass spectra, the SA fragments to a greater extent and to a greater number of product ions in the 266 nm MALDI mass spectra. In addition, although the m/z 207 fragment ion dominates in the 355 nm MALDI mass spectra, an intense m/z 180 fragment ion dominates all 266 nm MALDI mass spectra. Finally, in contrast to the CPT mass spectra, the expanded SA parent ion region shows that at 355 nm a large signal from the protonated SA is observed, whereas at 266 nm the $SA^{+\cdot}$ is the dominant matrix parent ion.

Protonated biomolecule ion signals are observed for

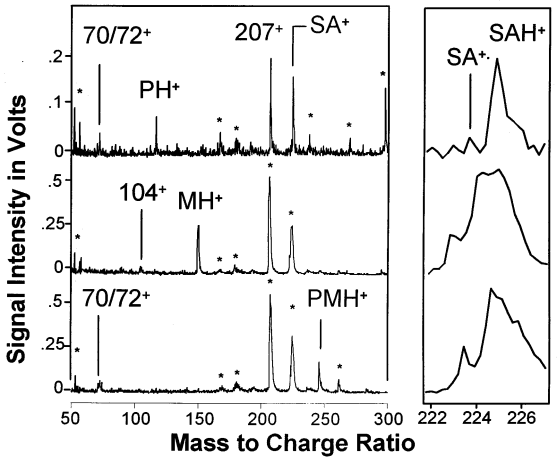

Figure 5. Positive ion 355 nm MALDI mass spectra of (**a**) proline, (**b**) methionine, and (**c**) prolylmethionine with sinapinic acid as the matrix. Each mass spectrum is the average of 50 laser shots taken at near threshold desorption energies. Expansion of the corresponding matrix parent ion region is shown to the right of each mass spectrum.

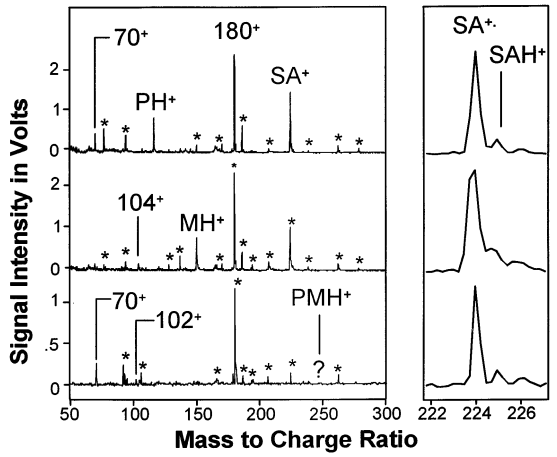

Figure 6. Positive ion 266 MALDI mass spectra of (**a**) proline, (**b**) methionine, and (**c**) prolylmethionine with sinapinic acid as the matrix. Each mass spectrum is the average of 50 laser shots taken at near threshold desorption energies. Expansions of the corresponding matrix parent ion region is shown to the right of each mass spectrum.

P and M in both 355 and 266 nm MALDI mass spectra. For PM the protonated dipeptide ion signal is only observed in the 355 nm MALDI mass spectrum. The 355 nm MALDI mass spectra of P and PM both show biomolecular fragment ion signals at m/z 70 and 72, whereas only the m/z 70 fragment ion signals are observed in the 266 nm MALDI mass spectra. Additionally, the fragment ion signal at m/z 70 increases in intensity relative to the protonated P and PM ion signals when going from 355 to 266 nm. The 355 and 266 nm MALDI mass spectra of M contain a wavelength independent signal at m/z 104. Both the m/z 70 and m/z 104 fragment ions result from decarboxylation of the parent biomolecule; a commonly observed fragmentation path in delayed extraction and postsource decay MALDI mass spectra. The observation of these ions as prompt fragments in the MALDI mass spectra presented may be a result of the lower matrix to analyte ratio used in our experiments.

Discussion

In general, the results of our studies indicate that MALDI matrix to biomolecule analyte CPT reactions can lead to substantial yields of protonated small biomolecules. Furthermore, studies performed in our laboratory have shown that polypeptides with molecular weights up to several thousand Da can be ionized via analogous CPT reactions. Thus, the CPT mechanism of analyte protonation appears viable as a contributor to the mechanism of analyte protonation during MALDI.

The laser power plots for the pure SA clearly suggest that the $SA^{+\cdot}$ is formed by a two photon ionization process at both 266 and 355 nm (see Table 1). The 266 nm result is important and demonstrates that the ionizing laser power plots for laser desorbed and jet entrained molecules produce results that are consistent with expected ionization energies between 7.0 and 9.0 eV for substituted aromatic molecules. Although the ionization energy for SA is unknown, ionization energies of 8.5 eV have been reported for other substituted cinnamic acid molecules [30]. Thus, the total two photon energy at 266 nm of 9.3 eV should readily ionize the SA to form $SA^{+\cdot}$. The total two photon energy at 355 nm of 7.0 eV appears somewhat low. However, this lower value could be sufficient if the ionization energy for SA is at the lower limit for aromatic molecules and/or if the ionization energy of SA is reduced in the cluster environment. The ionization energies of adenine and thymine can be reduced by 0.7 eV in hydrated clusters with the addition of as few as three water molecules [31]. For pure methyl amine clusters, the ionization energy decreases from 8.97 eV for the monomer to 7.9 eV for the trimer [32]. Finally, a nearly 2 eV reduction (from 8.50 to 6.68 eV) in the ionization energy of phenol is observed upon clustering with just five ammonia molecules [33]. Given that the clusters produced using the experimental methodology described can contain substantially more than five or six molecules, a 1.0 to 1.5 eV reduction in the ionization energy of SA is not unreasonable.

The two photon dependence for $SA^{+\cdot}$ formation is also supported in the ionization laser power plots for the coclustered SA+analyte systems. Note that the slopes of the power plots for the $SA^{+\cdot}$ given in Table 1 are generally between 1.5 and 2.0. In addition, the slopes of the ionization laser power plots for the three protonated analyte molecules are also predominately consistent with a two photon dependence for ion production. Of equal importance, the slopes of the plots of the ratio of the protonated analyte to $SA^{+\cdot}$ ion signals as a function of ionization laser power (see Table 2) show no systematic increasing or decreasing power dependence, i.e., the ratio of the protonated analyte ion signal to the $SA^{+\cdot}$ ion signal is essentially independent of the ionization laser power. These results suggest that the protonated analyte is formed at the same two photon dependence as the $SA^{+\cdot}$ and thus, that the $SA^{+\cdot}$ must act to transfer a proton to the analyte via dissociative CPT:

$$SA_xB_yAR_z \xrightarrow{2h\nu} [SA_xB_yAr_z]^{+\cdot} \rightarrow [SA - H]^{\cdot} + (x-1)SA + BH^+ + (y-1)B + zAr$$

In this mechanism, a clustered SA molecule first undergoes two photon ionization and then acts to transfer a proton to the coclustered biomolecule analyte (B). Subsequently, excess energy from either the initial photoexcitation or the enthalpy of the proton transfer reaction leads to partial and/or total dissociation of the cluster to form the observed protonated analyte ion signal.

Two other mechanisms of CPT must be considered unlikely in view of the experimental results. First, a protonated SA molecule can be ruled out as the primary proton donor (although it may be formed in the clusters

as a reactive intermediate) because the large positive potential bias on the source region excludes charged clusters from entering the TOFMS source region. Furthermore, although the slopes of the ionization laser power plots are reduced to values below 2.0, suggesting the possible contribution of a one photon excited state CPT ionization process, the lack of ion signals in the negative ion mass spectrum argues against this mechanism. In an excited state CPT mechanism the production of an $[SA - H]^-$ product ion would be expected:

$$SA_xB_yAr_z \xrightarrow{h\nu} [SA_xB_yAr_z]^* \rightarrow [SA - H]^- + (x - 1)SA + BH^+ + (y - 1)B + zAr$$

Indeed, the reduction in the slopes of the SA ionization laser power plots to values somewhat less than 2.0 is consistent with an interpretation based on the introduction of an alternate pathway for $SA^{+\cdot}$ depletion via proton transfer to the analyte molecule.

Comparisons Between CPT and MALDI Mass Spectra

It is of interest to note the similarities and differences in the wavelength dependent mass spectra produced by dissociative CPT and MALDI in order to evaluate the potential contribution of the CPT process to the MALDI ion formation mechanism. At both laser excitation wavelengths it appears that the extent of SA fragmentation is reduced in the CPT mass spectra as compared with the MALDI mass spectra. At 355 nm both the MALDI and CPT mass spectra contain SA fragment ions at m/z 207, but the yield of this fragment ion is substantially reduced in the CPT mass spectra. Kosaka and co-workers have recently investigated the fragmentation pattern of SA under various ionization conditions and attributed the m/z 207 fragment ion to dehydration of the protonated SA [34]. In agreement with the 337 nm MALDI mass spectra shown by Kosaka et al., our 355 nm MALDI mass spectra show a sizable signal from both the protonated SA and the m/z 207 fragment ion. In the 355 nm CPT mass spectra, however, the $SA^{+\cdot}$ is the dominant matrix parent ion and only small signals can be attributed to either the protonated SA or the m/z 207 fragment ion. Similar to the behavior of ferrulic acid [35], Kosaka et al. attributed the m/z 180 fragment ion observed in the 266 nm MALDI and CPT mass spectra to a decarboxylated thermal degradation product of the SA molecule [34]. Comparison of the m/z 180 ion signal intensity in the 266 and 355 nm MALDI mass spectra suggest that decomposition of the SA is substantially increased when using the 266 nm laser desorption wavelength. In contrast, the 266 nm CPT mass spectra show significantly reduced ion signals from the m/z 180 degradation product, and intense ion signals from both the $SA^{+\cdot}$ and the various protonated analyte molecules. Finally, significant differences exist in the wavelength dependent MALDI and CPT yields of protonated and radical cation SA ion signals. Overall, it must be concluded that there are both inconsistencies and similarities in the wavelength dependent SA ion signals produced by CPT and MALDI.

Comparison of the analyte ion signals in the wavelength dependent MALDI and CPT mass spectra also reveals both similarities and differences. In general, the extent of fragmentation of P and M is equivalent in the MALDI and CPT mass spectra at both excitation wavelengths. The comparison is less clear for PM because of the m/z 102 fragment ion in the 355 nm CPT and 266 nm MALDI mass spectra, and the absence of the protonated PM in the 266 nm MALDI mass spectrum. There is, however, a similarity in the wavelength dependent fragmentation of P and PM. At 355 nm both m/z 70 and m/z 72 fragment ions are observed in the mass spectra of P and PM, whereas at 266 nm only the m/z 70 fragment ion is observed. For M, the intensity of the fragment ion at m/z 104 relative to the protonated parent molecule is nearly identical at both wavelengths and when using either ionization method.

Conclusions

Our studies show that a MALDI matrix such as SA can act to efficiently protonate small biomolecules upon photoexcitation of mixed clusters of the two species. Investigation of the ionization laser power dependence for CPT from SA to several small biomolecular analytes suggests that two photons are required for both the formation of $SA^{+\cdot}$ and the protonated analyte at both 266 and 355 nm. This result is further confirmed by noting that the yield of the $SA^{+\cdot}$ relative to the protonated analyte is independent of the ionizing laser power. Interestingly, this result is in agreement with the observation by Dreisewerd et al. that the relative yields of protonated bovine insulin and $SA^{+\cdot}$ produced by MALDI are independent of ionizing laser power [36]. Furthermore, negative ion mass spectra have failed to reveal formation of the deprotonated matrix anions. Cumulatively these results support a mechanism of intracluster proton transfer in which the SA acid is first photoionized to form $SA^{+\cdot}$ which then transfers a proton to a coclustered biomolecule analyte. Subsequent dissociation of the cluster leads to the product ions observed in the mass spectrum.

The relative importance of a matrix to analyte CPT mechanism in MALDI is considerably less clear however. Although similarities in the matrix and analyte ion signals exist in the wavelength dependent CPT and MALDI mass spectra, discrepancies were also noted. These differences are manifested in both the relative yields of matrix radical cation and protonated matrix ion signals as well as in the yields and identities of the analyte fragment ions. In addition, the failure to observe the formation of negative ions is of significant concern since conventional MALDI mass spectra can

frequently be obtained in the negative ion mode. On the other hand, it is certainly premature to conclude that a CPT mechanism plays no role in the MALDI analyte ionization process. It is likely that MALDI analyte ionization involves a combination of condensed phase and gas phase processes, of which CPT may only play a small part. Further studies of the type described in this report should reveal to what extent and under what conditions the CPT mechanism plays a role in MALDI analyte ionization.

Acknowledgment

The authors gratefully acknowledge the financial support of the University of Texas at Arlington, Research Enhancement Program.

References

1. Karas, M.; Bachmann, D.; Bahr, U.; Hillenkamp, F. *Int. J. Mass Spectrom. Ion Processes* **1987,** *78*, 53–68.
2. Tanaka, K; Waki, H.; Ido, Y.; Akita, S.; Yoshida Y.; Yoshida, T. *Rapid Commun. Mass Spectrom.* **1988,** *2*, 151–153.
3. Hillenkamp, F.; Karas, M.; Beavis, R. C.; Chait, B. T. *Anal. Chem.* **1991,** *63*, 1193A–1203A.
4. Spengler, B.; Kaufmann, R. *Analysis* **1992,** *20*, 91–101.
5. Gimon, M. E.; Preston, L. M.; Solouki, T.; White, M. A.; Russell, D. H. *Org. Mass Spectrom.* **1992,** *27*, 827–830.
6. Chiarelli, M. P.; Sharkey, A. G., Jr.; Hercules, D. M. *Anal. Chem.* **1993,** *65*, 307–311.
7. Ehring, H.; Karas, M.; Hillenkamp, F. *Org. Mass Spectrom.* **1992,** *27*, 472–480.
8. Karas, M.; Bahr, U.; Strupat, K.; Hillenkamp, F.; Tsarbopoulos, A.; Pramanik, B. *Anal. Chem.* **1995,** *67*, 675–679.
9. Preston-Schaffter, L. M.; Kinsel, G. R.; Russell, D. H. *J. Am. Soc. Mass Spectrom.* **1994,** *5*, 800–806.
10. Jorgenson, R. J. D.; Vulpius, R.; Bojesen, G. *Abstracts of the 13th International Mass Spectrometry Conference*; Budapest, Hungary, 1994; p 175.
11. Ehring, H.; Sundqvist, B. U. R. *J. Mass Spectrom.* **1995,** *30*, 1303–1310.
12. Knochenmuss, R.; Dubois, F.; Dale, M. J.; Zenobi, R. *Rapid Commun. Mass Spectrom.* **1996,** *10*, 871–877.
13. Allwood, D. A.; Dyer, P. E.; Dreyfus, R. W. *Rapid Commun. Mass Spectrom.* **1997,** *11*, 499–503.
14. Burton, R. D.; Watson, C. H.; Eyler, J. R.; Lang, G. L.; Powell, D. H.; Avery, M. Y. *Rapid Commun. Mass Spectrom.* **1997,** *11*, 443–446.
15. Gimon-Kinsel, M.; Preston-Schaffter, L. M.; Kinsel, G. R.; Russell, D. H. *J. Am. Chem. Soc.* **1997,** *119*, 2534–2540.
16. Tang, X.; Sadeghi, M.; Olumee, Z.; Vertes, A. *Rapid Commun. Mass Spectrom.* **1997,** *11*, 484–488.
17. Ehring, J.; Costa, C.; Demirev, P. A.; Sundqvist, B. U. R. *Rapid Commun. Mass Spectrom.* **1996,** *10*, 821–824.
18. Zhou, J.; Ens, W.; Standing, K. G.; Verentchikov, A. *Rapid Commun. Mass Spectrom.* **1992,** *6*, 671–678.
19. Giannakopulos, A. E.; Reynolds, D. J.; Dominic Chan, R.-W.; Colburn, A. W.; Derrick, P. J. *Int. J. Mass Spectrom. Ion Processes* **1994,** *131*, 67–86.
20. Kinsel, G. R.; Edmondson, R. D.; Russell, D. H. *J. Mass Spectrom.* **1997,** *32*, 714–722.
21. Kinsel, G. R.; Gillig, K.; Edmondson, R. D.; Russell, D. H. *Presented at the 42nd ASMS Conference on Mass Spectrometry and Allied Topics*; Chicago, IL, June, 1994.
22. Bökelmann, V.; Spengler, B.; Kaufmann, R. *Eur. Mass Spectrom.* **1995,** *1*, 81–93.
23. Huang, Y.; Russell, D. H. *Proceedings of the 44th ASMS Conference on Mass Spectrometry and Allied Topics*; Portland, Oregon, May 12–16, 1996; p 1224.
24. Meffert, A.; Grotemeyer, J. *Eur. Mass Spectrom.* **1995,** *1*, 594–598.
25. Krutchinski, A. N.; Dolguine, A. I.; Khodorkovski, M. A. *Anal. Chem.* **1995,** *67*, 1963–1967.
26. Land, C. M.; Kinsel, G. R. *Proceedings of the 45th ASMS Conference on Mass Spectrometry and Allied Topics*; Palm Springs, California, June 1–5, 1997; p 850.
27. Land, C. M.; Kinsel, G. R. *Proceedings of the 44th ASMS Conference on Mass Spectrometry and Allied Topics*; Portland, Oregon, May 12–16, 1996; p 808.
28. Mafuné, F.; Hashimoto, Y.; Hashimoto, M.; Kondow, T. *J. Phys. Chem.* **1995,** *99*, 13814–13818.
29. Huang, Y.; Sulkes, M. *Chem. Phys. Lett.* **1996,** *254*, 242–248.
30. Schaldach, B. *Int. J. Mass Spectrom. Ion Processes* **1984,** *56*, 237–241.
31. Kim, S.; Lee W.; Herschbach, D. *J. Phys. Chem.* **1996,** *100*, 7933–7937.
32. Brutschy, B. *J. Phys. Chem.* **1990,** *94*, 8637–8647.
33. Jouvet, C.; Solgadi, D. *Chemical Reactions in Clusters*; Bernstein, E. R., Ed.; Oxford University Press: New York, 1996.
34. Kosaka, T.; Kinoshita, T. *Rapid Commun. Mass Spectrom.* **1996,** *10*, 405–408.
35. Huth-Fehre, T.; Becker, C. H. *Rapid Commun. Mass Spectrom.* **1991,** *5*, 378–382.
36. Dreiswerd, K.; Schürenberg, M.; Karas, M.; Hillenkamp, F. *Int. J. Mass Spectrom. Ion Processes* **1995,** *141*, 127–148.